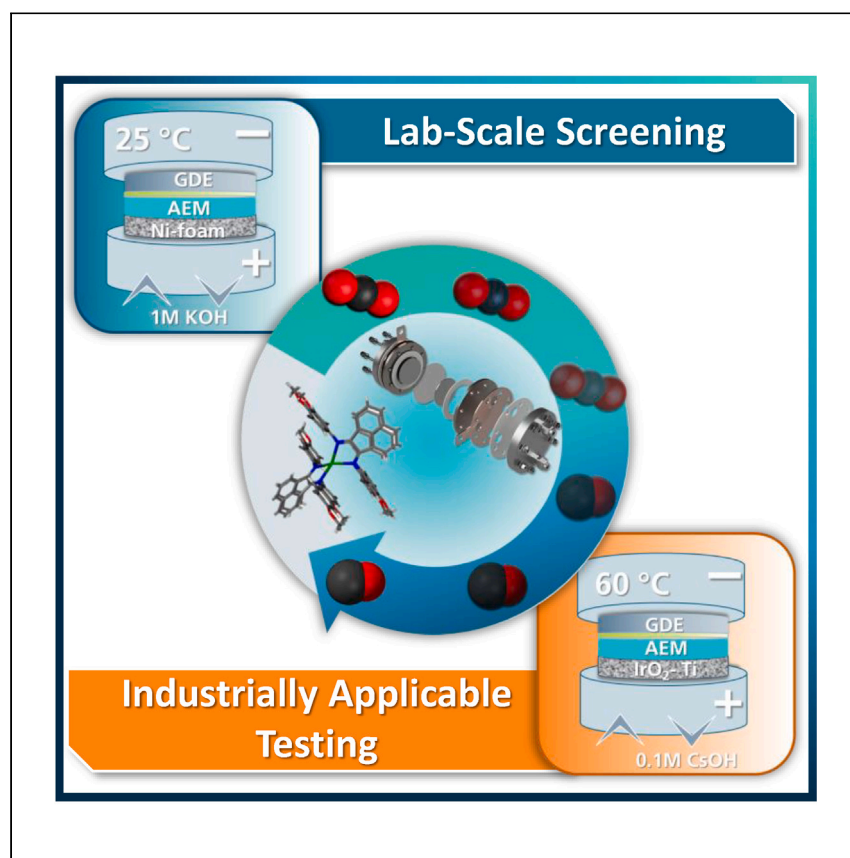


**Article**

# Pushing the Ag-loading of CO<sub>2</sub> electrolyzers to the minimum via molecularly tuned environments



Pellumbi et al. present a holistic pathway coupling molecular catalyst design and reactor optimization for CO<sub>2</sub> electroreduction. The dynamic interplay between CO<sub>2</sub> and mass flux is explored, allowing for rapid transition at different cell scales and elevated mass activity for CO production at current densities >300 mA cm<sup>-2</sup>.

Kevinjeorjos Pellumbi, Dominik Krisch, Clara Rettenmaier, ..., Beatriz Roldan Cuenya, Wolfgang Schöfberger, Ulf-Peter Apfel

wolfgang.schoefberger@jku.at (W.S.)  
ulf.apfel@rub.de (U.-P.A.)

## Highlights

Ag-BIAN catalysts are a highly mass-active class of CO<sub>2</sub> electrocatalysts

Catalyst aggregation plays an important role in observed activity

For each applied current density an ideal ratio between the CO<sub>2</sub> and H<sub>2</sub>O flow exists

Tailoring of the CO<sub>2</sub>/H<sub>2</sub>O ratio allows for faster transfer to larger cell designs



Article

# Pushing the Ag-loading of CO<sub>2</sub> electrolyzers to the minimum via molecularly tuned environments

Kevinjeorjios Pellumbi,<sup>1,2</sup> Dominik Krisch,<sup>3</sup> Clara Rettenmaier,<sup>4</sup> Houssein Awada,<sup>3</sup> He Sun,<sup>3</sup> Luyang Song,<sup>3</sup> Sebastian A. Sanden,<sup>2</sup> Lucas Hoof,<sup>1</sup> Leonard Messing,<sup>1</sup> Kai junge Puring,<sup>1</sup> Daniel Siegmund,<sup>1,2</sup> Beatriz Roldan Cuenya,<sup>4</sup> Wolfgang Schöfberger,<sup>3,\*</sup> and Ulf-Peter Apfel<sup>1,2,5,\*</sup>

## SUMMARY

Electrochemically converting CO<sub>2</sub> to renewable synthons is steadily becoming a globally scalable and important CO<sub>2</sub> utilization technology. Nevertheless, most industrial endeavors employ catalysts based on metallic Ag or Au, with few catalytically competitive alternatives, showing similar activity, high mass activity, and cost efficiency. Similarly, this effort is hindered by insufficient testing of promising materials in application-oriented conditions. We herein present a holistic pathway starting from the conceptualization of different Ag(I)-based molecular catalysts to their complete integration into directly industrially applicable cell assemblies. Notably, optimization of not only the catalyst but also the operational conditions allowed us to achieve CO<sub>2</sub> electrolysis for at least 110 h at 300 mA cm<sup>-2</sup> and 80 h at 600 mA cm<sup>-2</sup> with an FE<sub>CO</sub> decay rate of 0.01% h<sup>-1</sup>. Beyond significant mass activity improvements for CO production, we provide the community with a broad toolbox toward improving catalytic and cell performance directly between different cell sizes.

## INTRODUCTION

Creating a closed carbon cycle powered by renewable sources is considered the key to a fossil-fuel-independent future. Here, electrocatalytic CO<sub>2</sub> conversion is a highly promising route toward the generation of important carbon synthons such as carbon monoxide, formic acid, methanol, or even multi-carbon products.<sup>1–3</sup>

Among the multitude of possible products from the electroreduction of CO<sub>2</sub>, the conversion of CO<sub>2</sub> to CO constitutes the most advanced cathodic process.<sup>4–8</sup> Mainly performed via the use of heterogeneous catalysts based on Ag and Au, significant efforts in recent years have been focused on increasing the mass activity of the generated catalytic layers while maintaining selectivity at elevated current densities, either through complexation with N-containing molecules or smart engineering of the catalytic morphology/layer (>300 mA cm<sup>-2</sup>).<sup>9–14</sup>

Simultaneously, ligand engineering is one of the key components of active molecular electrocatalysts (MECs) for electrochemical CO<sub>2</sub> reduction (CO<sub>2</sub>R). Notably, by carefully adjusting the steric and electronic properties of the ligand environment around a metal center, crucial parameters, such as the flux of water, CO<sub>2</sub>, and electrons to the catalytic centers, can be tuned toward optimal CO<sub>2</sub>R activity and product selectivity.<sup>15–21</sup>

<sup>1</sup>Fraunhofer Institute for Environmental, Safety and Energy Technology UMSICHT, Osterfelderstraße 3, 46047 Oberhausen, Germany

<sup>2</sup>Inorganic Chemistry I, Ruhr University Bochum, Universitätsstraße 150, 44780 Bochum, Germany

<sup>3</sup>Institute of Organic Chemistry, Laboratory for Sustainable Chemistry and Catalysis (LSusCat), Johannes Kepler University (JKU), Altenberger Straße 69, 4040 Linz, Austria

<sup>4</sup>Department of Interface Science, Fritz-Haber Institute of the Max Planck Society, 14195 Berlin, Germany

<sup>5</sup>Lead contact

\*Correspondence:  
[wolfgang.schoefberger@jku.at](mailto:wolfgang.schoefberger@jku.at) (W.S.),  
[ulf.apfel@rub.de](mailto:ulf.apfel@rub.de) (U.-P.A.)

<https://doi.org/10.1016/j.xrps.2023.101746>



We thus turned the focus of our application-oriented approach toward the integration of easily tunable ligand systems that can be synthesized in a facile manner similarly to their reported Ag-N coordinated counterparts. Here, we envisioned that the bis(arylimino)acenaphthene (BIAN) system could provide a ligand scaffold satisfying the previously set requirements. With BIAN ligands being reported mainly in thermocatalytic reactions, with few insights into their electrocatalytic performance, their large-scale synthesis (up to 100-g scale) was demonstrated.<sup>22,23</sup> Most importantly, their preparation through, e.g., green and rapidly scalable mechanochemical methods has been reported, showing its promising perspective toward industrial adoption against reported MECs and single-atom catalysts that in some cases require multiple synthetic steps.<sup>24</sup> In addition, elevated tunability is another major advantage of the BIAN structure. Here, the interesting ability of the BIAN ligand to accept electrons as well as to functionalize the imine moieties adjacent to the metal center offers exciting possibilities toward generating efficient and highly tunable electrocatalysts at the molecular level.<sup>25</sup>

Notably, while novel electrocatalysts are being reported in rapid fashion, most industrial endeavors mainly employ Ag- or Au-based gas-diffusion electrodes (GDEs) in scaled-up electrolyzers for the CO<sub>2</sub>-to-CO conversion. From our perspective, the adoption of novel materials by CO<sub>2</sub>-focused projects on the industrial level is limited not only to the catalytic cost against the state of the art but also the employed electrochemical testing parameters. Specifically, novel materials and the associated cells are rarely tested in industrially relevant environments involving higher temperatures (60°C–80°C), significantly diluted electrolytes, and the application of elevated current densities for hundreds of hours.<sup>26,27</sup> In case of ligated electrocatalysts, no investigations have been performed on how to precisely improve tailored operational parameters (gas humidity, flow rate) to better fit their specific needs.

We therefore set out not only to test different electrocatalytic structures but to create a holistic pathway in which instead of focusing on improving individual components, we transition rapidly from electrocatalytic screening to industrially applicable cells tailoring the respective key components along the way. This component optimization is spread across the whole material/cell chain, including tuning of the ligand environment, ink composition, cell parameters, and material selection, aiming to generate a holistically optimized system.<sup>15,28–30</sup> Throughout this process, postmortem analysis of the generated electrodes became a fundamental goal of our approach, essentially setting the question: when focusing on industrial application, which optimization point possesses the highest significance—the catalyst, the electrode structure, or the operational parameters?

Here we present for the first time a complete pathway from the conceptualization of a molecular electrocatalyst to its full-scale optimization in an industrially relevant cell design. Along the way, we present key tuning points toward increasing the selectivity and efficiency for CO and syngas generation. Our aggregate Ag(I)-BIAN system can compete with classical Ag-based systems in directly industrially adoptable cell concepts at current densities close to the A cm<sup>-2</sup> level to produce tunable CO/H<sub>2</sub> mixtures. Furthermore, the design strategy presented herein allows us to reach the highest mass activity reported so far for CO with Ag-containing catalytic layers (101,636 mA mg<sub>Ag</sub><sup>-1</sup>). Coupled with *in situ* and *ex situ* postmortem measurements, we clearly demonstrate that the electrocatalyst is only one piece of a highly dynamic and tunable puzzle as the technological readiness level is gradually increased.

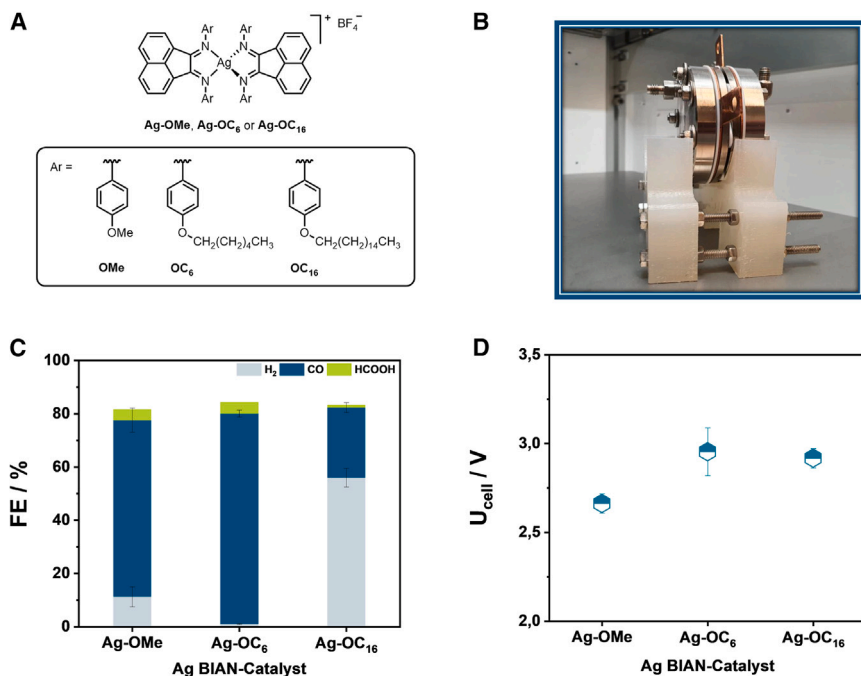


**Figure 1. Influence of the ligand environment on the CO<sub>2</sub> reduction activity in zero-gap electrolyzers**

(A) Structure of the Ag(I) bis-BIANS catalysts used in this work.  
 (B) Image of the employed zero-gap electrolyzer in this work.  
 (C and D) Faradic efficiencies for the different Ag complexes at 100 mA cm<sup>-2</sup> at a loading of 0.5 mg cm<sup>-2</sup> of catalyst after 1 h of electrolysis (C) and the respective cell voltages (D). Error bars represent the standard deviation from three separate measurements.

## RESULTS AND DISCUSSION

### Design strategy behind the synthesized Ag(I)-BIAN complexes and developed electrodes

Among the different approaches toward improving the activity and selectivity of molecular electrocatalysts, such as immobilization on conductive supports,<sup>17,28,31,32</sup> adjustment of the function of pendant groups,<sup>33,34</sup> and functionalization of the ligand structure,<sup>35–38</sup> the integration of electron-donating as well as hydrophobic groups appears to present one of the most promising and straightforward pathways toward catalytic optimization. Here, by taking advantage of the synthetic flexibility of BIAN ligands to directly alter the local environment around the Ag catalytic center through the modified *N,N'*-bis(arylimino)acenaphthene moieties, we integrated alkyl chains of different lengths at the phenyl ring, ranging from methoxy- (Ag-OMe), to hexyloxy- (Ag-OC<sub>6</sub>), and finally hexadecyloxy- (Ag-OC<sub>16</sub>) substituents (Figure 1A). Additional information on the synthesis and characterization of the Ag-BIANS can be found in the supplemental experimental procedures and Figures S47–S79, respectively.

Notably, regarding our GDE architecture, we aimed to minimize and simplify the preparation steps toward the generation of a large-scale fabricable GDE. Specifically, carbon black (ENSACO 250G) was employed as an inexpensive carbon support, free of possible metal impurities compared to carbon nanotubes, being directly mixed with the molecular electrocatalysts under investigation at an Ag-BIAN loading of 0.5 mg cm<sup>-2</sup>. We specifically selected ethanol as our main ink component, abstaining from high-boiling-point solvents such as dimethylformamide, often used for the dispersion of molecular electrocatalysts, to align our

investigation with the standards set by industrial endeavors in the field of CO<sub>2</sub> reduction.<sup>39</sup> The result is a non-specifically nanostructured catalytic layer (Figures S2 and S3). While nanostructured electrodes, via tailored impregnation techniques, have shown notable performance improvements in multiple cases,<sup>20,40–44</sup> we believe that our simple GDE architectures ensure, at least in initial upscaling stages, a reproducible and easily transferable GDE in the m<sup>2</sup> range via automated methods.

#### Integration of the Ag(I)-BIAN complexes in lab-scale zero-gap electrolyzers

For our electrocatalytic screening, we performed a parallel testing of the synthesized Ag-BIAN electrodes in both H-type and industrially relevant, zero-gap electrolyzers (ZGEs) to better understand bringing points and gaps between the two screening methods. On the one hand, H-type investigations aim to provide information regarding possible structure-activity trends as well as mechanistic insights for the different catalysts, without the introduction of additional contributions from the operational parameters of the ZGE or electrode structure. On the other hand, our ZGE investigations aim to test the perspective of these novel Ag-BIAN catalysts for CO<sub>2</sub>R. Specifically, H-type cell experiments were performed in acetonitrile for Ag-OMe and Ag-OC<sub>6</sub>, while due to solubility issues Ag-OC<sub>16</sub> could only be investigated in tetrahydrofuran (THF). For our initial testing in ZGEs, we applied a constant current density of 100 mA cm<sup>-2</sup> for 1 h under ambient conditions. Here, parallel titanium flow fields ensured the transport of wetted CO<sub>2</sub> (100% relative humidity) to the catalytic centers as well as of the 1 M KOH anolyte to anode. During this screening we employed Ni foam as the anode material for the oxygen evolution reaction, with the two electrodes being separated by a Sustainion anion-exchange membrane (Figures 1B and S1). Such a setup allows for a facile evaluation of catalytic performance prior to transitioning to an industrially applicable fine-tuning stage toward higher current densities.

H-type cell tests in argon-containing electrolytes reveal for both pure ligands and complexed compounds the non-innocent nature of the synthesized BIAN ligands. During cyclovoltammetry a first reduction peak is observed at ca. -0.7 V vs. normal hydrogen electrode (NHE), which indicates a BIAN radical anion formation. The second peak observed at larger cathodic potentials, -1.1 V vs. NHE for Ag-OC<sub>6</sub> and -1.5 V vs. NHE for Ag-OC<sub>16</sub>, can be assigned to a full reduction in the respective BIAN anion ligands (Figures S4–S7).<sup>45</sup> Consequently, this ability enables the two iminoaryl parts of the homoleptic Ag-BIAN complexes to act as electron reservoirs during the electroreduction process, constantly supplying electrons to the metal center. This electron-funneling ability facilitates the two consecutive proton-coupled electron transfer (PCET) steps during the CO<sub>2</sub>-to-CO reduction process, underlining the growing consensus that ligand systems do not merely adjust electronic and geometric environments but can also play a pivotal activity role in CO<sub>2</sub> electrocatalysis.<sup>22</sup>

During our H-type investigation, all catalysts underwent testing in a dissolved state. Given that contributions from our 0.28-cm<sup>2</sup> carbon working electrode cannot be entirely ruled out, particularly under reductive potentials, we have chosen to exclusively present the attained current in microamperes (μA). This approach aims to facilitate a more accurate and meaningful comparison across the various solvents utilized in our study. Here, Ag-OC<sub>6</sub> greatly outperforms its other MeCN soluble counterpart Ag-OMe, reaching current values of 938 and 251 μA at -1.90 V vs. NHE, respectively (Figures S8–S16). Consequently, in THF, Ag-OC<sub>16</sub> demonstrates almost double the current value of its hexyloxy-functionalized counterpart, 85.7 vs. 55.4 μA. Subsequent gas chromatography measurements for Ag-OC<sub>6</sub> obtained at -2.0 V vs. reversible hydrogen electrode confirmed its reactivity, reaching a CO faradic efficiency

( $\text{FE}_{\text{CO}}$ ) value of ca. 40% (Figure S17 and Table S1). Similarly, to many monometallic MECs, CO appears to be the main product of the Ag-BIAN catalysts.<sup>17,46,47</sup> While here solubility issues do not allow for the direct comparison of the presented catalysts, their selectivity trends hint at an increase of the  $\text{CO}_2\text{R}$  activity toward CO, with increasing length of the alkyl chain.

These trends are only partly mirrored in the results obtained from the zero-gap approach. Under the aforementioned conditions and at  $100 \text{ mA cm}^{-2}$ , the Ag-OMe GDEs reach  $\text{FE}_{\text{CO}}$  values of 66%, while the Ag-OC<sub>6</sub> complex decreases the parasitic H<sub>2</sub> evolution to a value of 1% accompanied by an  $\text{FE}_{\text{CO}}$  of 80%, almost double the  $\text{FE}_{\text{CO}}$  value compared to the H-type cell experiments (Figure 1C). This again shows how the  $\text{CO}_2$  reduction abilities of MECs can be augmented using GDEs and their associated advantages, including the improvement of  $\text{CO}_2$  mass transport and better electron conductivity to the catalytic centers as well as overcoming solubility issues in organic electrolytes. Surprisingly, the incorporation of longer alkyl side chains leads to an abrupt decrease of the  $\text{FE}_{\text{CO}}$  to 25%. We attribute this severe increase toward H<sub>2</sub> evolution to the diminished dispersibility of Ag-OC<sub>16</sub> within the porous carbon matrix. While Ag-OC<sub>6</sub> appears to be fully incorporated with our amorphous carbon and in some cases particles of the reddish Ag-OMe catalyst are visible on the surface of the GDE, Ag-OC<sub>16</sub> forms a thick layer on the gas-diffusion layer surface, hindering  $\text{CO}_2$  and electron transport (Figures S18 and S19). Attempts to improve the dispersibility of Ag-OC<sub>16</sub> within the carbon matrix through the employed dispersion solvent, such as ethanol, 2-propanol, or hexane, did not yield any major improvements (Figures S20 and S21). Such trends are in line with recent reports showing that aggregation effects play a detrimental role in achieving high catalytic stability and selectivity in both transition metal and molecular electrocatalysts, since the accessibility of the active centers is limited due to low electrical conductivity and increased particle agglomeration.<sup>28,40</sup> Evidently, even though the role of pendant groups on the catalytic  $\text{CO}_2$ -reducing activity of molecular electrocatalysts has been previously investigated,<sup>48,49</sup> when transitioning from lab-scale screening results the overall electrode architecture and ink composition appears to majorly influence the observed activity, showing that H-type and zero-gap cell transferability cannot always be easily ensured.

While in H-type cells catalytic differences can be easily observed, this is not the case for ZGEs. Specifically, regarding the cell voltages, Ag-OMe shows the lowest value at 2.6 V followed by Ag-OC<sub>6</sub> and Ag-OC<sub>16</sub>, both lying at 2.9 V at  $100 \text{ mA cm}^{-2}$ . Here, clear electrocatalytic distinctions between the different Ag-BIAN catalysts possibly are masked by the multitude of ongoing processes within the zero-gap electrolyzer. The elevated cell-voltage values as well as the <90% total FE value can be attributed to the Ni-foam anode, which limits an optimized pressure distribution and a leak-free operation between the anode and the cathode in our current electrolyzer concept, a topic we will address subsequently in this article as we move toward more optimized systems (Figure 1D).

### Electrochemical $\text{CO}_2$ conversion in industrially applicable cell assemblies

Having demonstrated the activity of Ag-BIAN complexes to produce CO, we transitioned to testing in demonstrator-scale relevant conditions. While Ni-foam-based anodes fed with 1 M KOH present some cost-efficiency advantages during initial catalytic testing, the employment of elevated KOH concentrations can lead to an underestimation of the realistic cell voltages while also promoting the loss of  $\text{CO}_2$  through carbonate formation in the anolyte.<sup>50</sup> Ni-foam anodes have in this regard been shown to be unstable under such conditions, as the pH value of the anolyte draws closer to neutral.<sup>51</sup> In addition, the elevated K<sup>+</sup>-ion concentration can

promote carbonate buildup in the cathode through unintended cation crossover from the anion-exchange membrane.<sup>52</sup> Therefore, instead of Ni foam and 1 M KOH, we employed IrO<sub>2</sub>-coated Ti felts with 0.1 M CsOH as anolyte, based on previously reported optimized systems.<sup>8,53</sup> Simultaneously, the operational temperature was increased from 25°C to 60°C, employing in this case PiperION membranes that can withstand this electrolytic environment.<sup>8,53,54</sup> Maintaining our conveniently accessible electrode architecture, the prepared GDEs of our most active electrocatalyst, Ag-OC<sub>6</sub>, also showed increased CO selectivity in our industrially relevant setup, demonstrating an FE<sub>CO</sub> value of 65% at 300 mA cm<sup>-2</sup> (Figure 2A). Notably, small tweaks in the properties of electrolyzer parts can have significant effects on the observed activity.<sup>55</sup> Specifically, by employing a serpentine flow field instead of a parallel one, we achieved elevated FE<sub>CO</sub> values of 60% and 90% for Ag-OC<sub>6</sub> loadings of 0.02 mg cm<sup>-2</sup> and 0.5 mg cm<sup>-2</sup>, respectively (Figures 2A and S22). These values constitute an important breakthrough in terms of not only achieved selectivity but also breaking through the 200 mA cm<sup>-2</sup> barrier for MECs at an appreciable time-scale of 1 h. Surprisingly, in a direct comparison of similarly prepared cobalt phthalocyanine (CoPc)- and Ag-based GDEs, FE<sub>CO</sub> values of only 11% and 60%, respectively could be obtained (Figure S23). These values are below our expectations according to current reports in the literature.<sup>28,53</sup> Further investigation of this behavior showed that our carbon/Nafion-based ink composition led to the agglomeration of the CoPc and Ag nanoparticles. This trend is visible by the naked eye but was also confirmed by scanning electron microscopy and energy-dispersive X-ray spectroscopy (SEM-EDX) (Figures S18 and S24). This comparison again highlights the need to not just simply employ active CO<sub>2</sub>R electrocatalysts but also carefully tailor the ink recipe, employed binder, and additive content to the respective catalytic centers. While this remark has been highlighted in recent literature, it often constitutes an overlooked parameter. A clearer comparison of the performance of the Ag-OC<sub>6</sub> against the literature benchmark is therefore discussed further.

### Optimization of the electrolyzer operation parameters

In recent years, it has been clearly shown that achieving higher partial current densities is not only a matter of possessing highly active electrocatalysts but also tuning the reactive environment around them. Notably, the required molar excess of CO<sub>2</sub> ( $\lambda_{\text{CO}_2}$ ) and water ( $\lambda_{\text{H}_2\text{O}}$ ) as well as their respective ratio to favor the CO<sub>2</sub>R at different current densities have become crucial and often overlooked parameters during the reduction of CO<sub>2</sub>.<sup>56</sup> Notably in the case of MECs and ligand-coordinated systems, reports are limited, and clearly understanding their impact on catalytic activity is crucial toward developing an industrially relevant system. Similarly, recent results have shown how the employed binder can not only affect the morphology of the catalytic particles' architecture but also control the catalytic microenvironment by tuning the effect of interfacial water as well as accelerating the transport of ionic species such as OH<sup>-</sup>, CO<sub>3</sub><sup>2-</sup>, and HCO<sub>3</sub><sup>-</sup>.<sup>53,57</sup>

Specifically, with the help of our previously reported temperature-controlled setup and bubbler, we adjusted not only the  $\lambda_{\text{CO}_2}$  but also the  $\lambda_{\text{CO}_2}/\lambda_{\text{H}_2\text{O}}$  ratio. Notably, we are able to demonstrate that for each tested current density (300, 600, and 900 mA cm<sup>-2</sup>) an optimal  $\lambda_{\text{H}_2\text{O}}$ , i.e., relative humidity of CO<sub>2</sub>, exists, with the obtained trends demonstrating that the required  $\lambda_{\text{H}_2\text{O}}$  must be increased accordingly as higher current densities are targeted (Figure S25). Transitioning from a  $\lambda_{\text{CO}_2}/\lambda_{\text{H}_2\text{O}}$  ratio value of 1.2 to 2.5, while maintaining a constant  $\lambda_{\text{CO}_2}$  value of 6, leads to an FE<sub>CO</sub> increase of ca. 15% to a FE<sub>CO</sub> value of 51% at 600 mA cm<sup>-2</sup>. Further increase of the water content in the CO<sub>2</sub> stream leads to a decrease of the FE<sub>CO</sub> to 44%, showing that such operational parameters lie on a very fine balance. Subsequently,

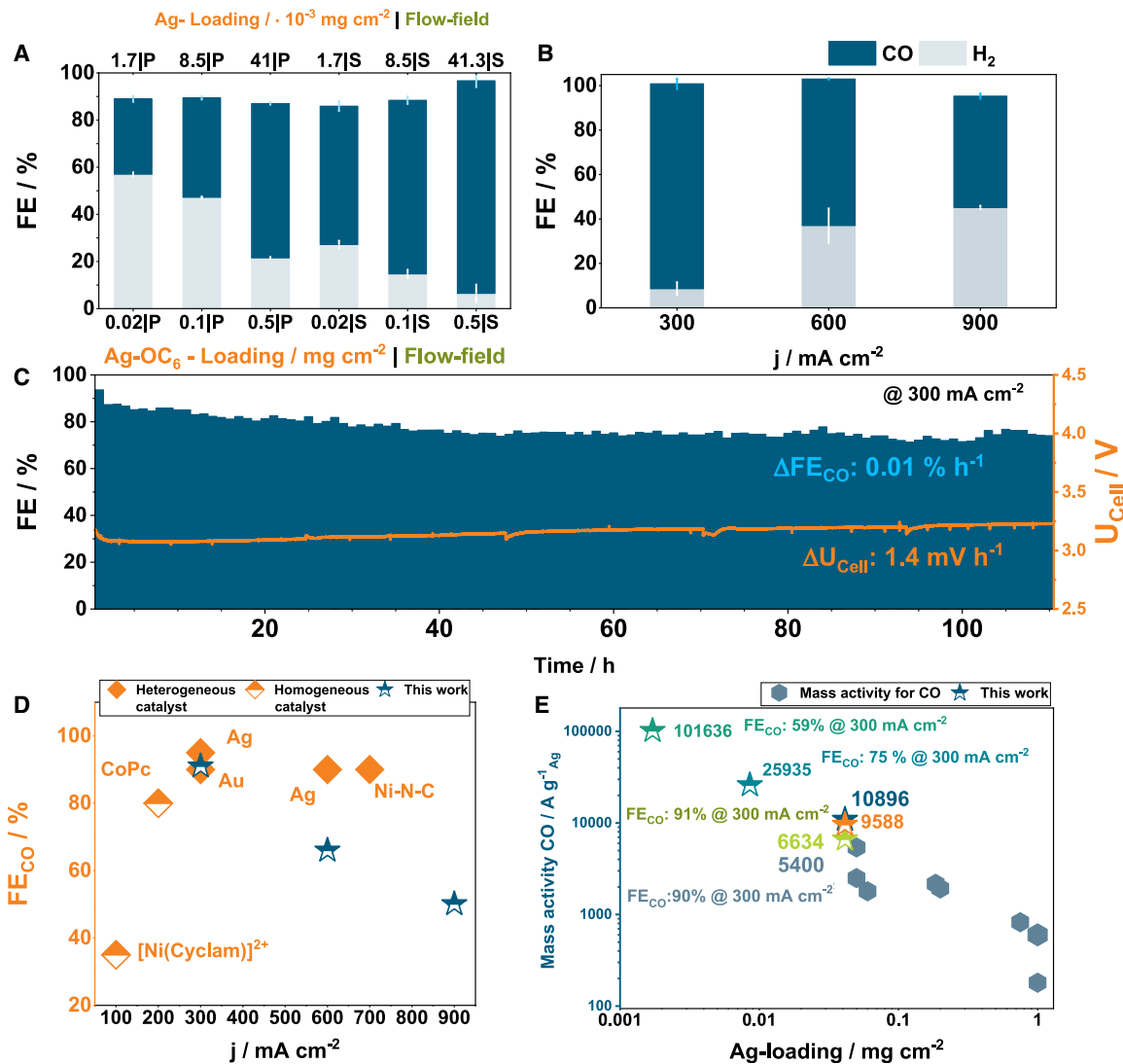


**Figure 2. Establishing Ag-BIAN GDEs in industrially applicable electrolyzers**

(A) Effect of the employed Ag-BIAN loading and flow field (S, serpentine; P, parallel) at  $300 \text{ mA cm}^{-2}$  and  $60^\circ\text{C}$  after 1 h of electrolysis.

(B) Current density variation at optimized  $\text{CO}_2$  flow rates and humidification values with an Ag-BIAN loading of  $0.5 \text{ mg cm}^{-2}$  using a serpentine flow field after 1 h of electrolysis.

(C) Long-term measurement of a PiperION-bound GDE with  $0.5 \text{ mg cm}^{-2}$  of  $\text{Ag-OC}_6$  using a serpentine flow field at  $300 \text{ mA cm}^{-2}$  at  $60^\circ\text{C}$ ; here the employed anolyte was  $0.05 \text{ M CsOH}$ .

(D and E) Comparison of the results presented herein with the state-of-the-art literature in terms of achieved  $\text{FE}_{\text{CO}}$  depending on the applied current density in zero-gap electrolyzers. (E) Comparison of the results presented herein with the state-of-the-art literature in terms of achieved mass activity for CO per loading of silver in zero-gap electrolyzer.<sup>9–14</sup>

Error bars represent the standard deviation from three separate measurements.

by maintaining the optimal  $\lambda_{\text{H}_2\text{O}}$  values, we varied the  $\lambda_{\text{CO}_2}$  value, aiming to find an optimal point between the required molar excess of  $\text{CO}_2$  and single-pass conversion (SPC)/FE to produce CO. For all three current densities, the higher the  $\lambda_{\text{CO}_2}$  value, the larger the obtained  $\text{FE}_{\text{CO}}$ , reaching values of 95% at  $300 \text{ mA cm}^{-2}$  and 40% at  $900 \text{ mA cm}^{-2}$  (Figure S26). Nevertheless, the use of elevated  $\text{CO}_2$  excess leads also to low SPC values below 10%, while in contrast using minimal  $\lambda_{\text{CO}_2}$  values of 3 leads to the SPC values of 29%, lying close to target SPC values for real-life applications (Table S2).<sup>53,58,59</sup>

Switching from Nafion to the anion-exchange ionomers Sustainion (XA-9) and PiperION (A5) allowed us to further improve our obtained performance. Here, PiperION-bound GDEs delivered higher performance, allowing us to reach partial current densities for CO of  $396 \text{ mA cm}^{-2}$  and  $450 \text{ mA cm}^{-2}$  at  $600 \text{ mA cm}^{-2}$  and  $900 \text{ mA cm}^{-2}$  after 1 h of electrolysis, respectively (Figures 2B and S27). Going beyond the 1-h experiments, our PiperION-bound Ag-OC<sub>6</sub> GDE, in our optimized environment, is able to operate for at least 110 h at  $300 \text{ mA cm}^{-2}$  and for at least 50 h at  $600 \text{ mA cm}^{-2}$ , maintaining an FE<sub>CO</sub> of 75% and 40% and a cell voltage of 3.1 V and 3.5 V, respectively after initial conditioning (Figures 2C and S28).<sup>54</sup> Notably, this process proceeds without the involvement of any cell or GDE washings (Figure 2C). Likewise, no carbonate salt formation is visible on the backside of the GDE or flow field after disassembly (Figure S29). This positive effect can be attributed to tailoring the incoming water flux through our bubbler to allow for performance in CO<sub>2</sub>RR and dissolution of formed carbonate crystals without leading to GDE flooding. Another decisive factor for this long-term stability was the choice of CsOH as the anolyte, with Cs-carbonate crystals being easier to dissolve than their K<sup>+</sup> counterparts.<sup>60,61</sup>

Finally, to show the transferability of our parameter optimization in different reactor sizes, we transitioned from a 2-cm<sup>2</sup> electrode area (16 mm diameter) to a 12.6-cm<sup>2</sup> active electrode area (40 mm) performing consecutive electrolytic experiments at  $300 \text{ mA cm}^{-2}$  with varying  $\lambda_{\text{CO}_2}/\lambda_{\text{H}_2\text{O}}$  ratios.<sup>5,60</sup> Notably, by transitioning from a  $\lambda_{\text{H}_2\text{O}}$  value of 3.5 to 1.8, at equal  $\lambda_{\text{CO}_2}$  values of 2.8, outlet mixtures of H<sub>2</sub>/CO ratios of ca. 1:1 and 1.5:1 could be generated, with 20 vol. % of CO being contained in the outlet stream (Figure S30). After a conditioning period, the system maintains overall a cell voltage of 3.6 V at  $300 \text{ mA cm}^{-2}$ . Similarly, even when employing only  $0.1 \text{ mg cm}^{-2}$  of Ag-OC<sub>6</sub>, an SPC to CO of 32% at FE<sub>CO</sub> values of 66% at  $240 \text{ mA cm}^{-2}$  (Figure S31) can be obtained. Although the generation of syngas by coupled CO<sub>2</sub>-to-CO and H<sub>2</sub>-producing systems is currently more cost and energy efficient than its direct generation by CO<sub>2</sub>R, our results again underline the often overlooked role of the water content in membrane-electrode assemblies to shift the product spectrum toward the CO<sub>2</sub>R in ZGEs.<sup>60</sup>

### Comparison with the current state of the art

Comparing the complexes presented herein with current Ag-based GDEs, we demonstrate the competitive selectivity for CO as well as syngas production at significantly decreased catalytic loadings using a molecular complex. Notably, regarding mass activity per Ag center contained in the catalytic layer, we present a significant improvement in terms of mass activity for generation of CO, ranging from  $6,634 \text{ mA mg}^{-1}_{\text{Ag}}$  to  $101,636 \text{ mA m g}^{-1}_{\text{Ag}}$  depending on the employed loading. Although lower catalytic loadings lead to the emergence of the hydrogen evolution reaction (HER), a catalytic loading of  $0.1 \text{ mg cm}^{-2}$  of Ag-OC<sub>6</sub> (Ag:  $8.5 \times 10^{-3} \text{ mg cm}^{-2}$ ) appears to lie close to the optimal point between elevated CO selectivity (FE<sub>CO</sub>: 75%) and mass activity ( $25,935 \text{ mA mg}^{-1}_{\text{Ag}}$ ), (Figures 2D, 2E, and S32).<sup>4,9–11,53,62</sup> Possibly, further tuning the operational conditions to such low catalytic loadings and thinner catalytic layers could lead to the further decrease of the parasitic HER. Moreover, the presented electrodes possess energy efficiencies comparable to both the current molecular and heterogenous state of the art, with energy-efficiency values lying at 51% (Tables S3 and S4). In terms of turnover frequency (TOF) (site<sup>-1</sup> h<sup>-1</sup>), the optimized Ag-OC<sub>6</sub> GDEs are able to reach a value of 21,156 at a loading of  $0.5 \text{ mg cm}^{-2}$ , with the value further increasing to 206,980 at the lowest tested loading of  $0.02 \text{ mg cm}^{-2}$ , belonging to some of the most active single-atom catalysts in the field of CO<sub>2</sub>R (Table S5).<sup>63,64</sup> This elevated

activity could be attributed to the non-innocent nature of the BIAN ligand acting as an electron reservoir during electrocatalysis, facilitating the performance of the PCET steps during the catalytic cycle, as supported by our accompanying density functional theory studies (Figures S33–S37 and Tables S5–S7). Such non-innocence effects are becoming ever more important in CO<sub>2</sub> electrocatalysis with molecular systems.<sup>65–67</sup>

Furthermore, in our opinion novel electrocatalysts that aim toward industrial applicability must not only demonstrate elevated FE<sub>CO</sub> and partial current density ( $j_{CO}$ ) values but also be obtainable by scalable methods in a cost-efficient manner. Here, we compared the euro-per-gram price of our Ag-OC<sub>6</sub> catalyst against Ag-NPs and Ni-N-C and the required catalytic loading to reach a  $j_{CO}$  value of 300 mA cm<sup>-2</sup> (Table S8).

Although our cost calculations only represent rough estimates, it is evident that both catalytic classes (Ag-BIAN and Ni-N-C) present highly interesting perspectives for the industrially focused CO<sub>2</sub>R field. We would therefore like to highlight the need for collaboration between both academic and commercial partners to push these catalysts into commercial availability, ensuring their eventual real-life applicability.

Overall, as evidenced by the comparative graph in Figure 2D, further fine-tuning of both catalytic structures and operational parameters is required for molecular systems to directly compete with heterogeneous catalysts, regarding the minimization of the parasitic HER in CO-focused scenarios, at current densities beyond 300 mA cm<sup>-2</sup>.

#### Postmortem and *in situ* analysis

Understanding changes in the structure of MECs can not only reveal information on possible morphological changes and catalytic reconstruction but also provide insight into the active catalytic species. In contrast, the use of a zero-gap electrolyzer often limits insights due to the delamination of the catalytic layer and design of the reactors, requiring the development of specialized cells to truly gain insights into the concurrent processes. To compensate for these limitations, we employed a combination of *ex situ* as well as quasi-*in situ* techniques, either by investigating the obtained GDEs directly after electrolysis, by dissolving the bound Ag-BIAN catalyst with the help of EtOH, or by performing quasi-*in situ* X-ray photoelectron spectroscopy (XPS) measurements to gain a clear understanding of the processes in an electrolyte environment.<sup>68</sup>

Starting with our *ex situ* investigations, our SEM-EDX analysis does not clearly show the formation of agglomerated particles or metallic films, while the powder X-ray diffraction analysis demonstrates that the electrodes presented herein show reflexes that can be attributed to metallic Ag after 1 h at 300 mA cm<sup>-2</sup> in our zero-gap electrolyzer (Figures S38–S40). In contrast, by dissolving the tested GDE-bound Ag-BIAN in EtOH, the obtained electrospray ionization-mass spectrometry and infrared spectra reveal the existence of the bound Ag(I) species, while surface analysis of a tested GDE via XPS demonstrates both the existence of the Ag(0) and Ag(I) species, confirming the stability of the Ag-bound iminoaryl ligands (Figures S41–S44 and Table S9). Furthermore, inductively coupled plasma-optical emission spectrometry investigations showed no crossover of Ag species within the detection limits of our apparatus (Table S10).

Most importantly for our postmortem analysis, we also specifically performed XANES and XPS analysis of our long-term tested (110 h) GDE sample. Interestingly,

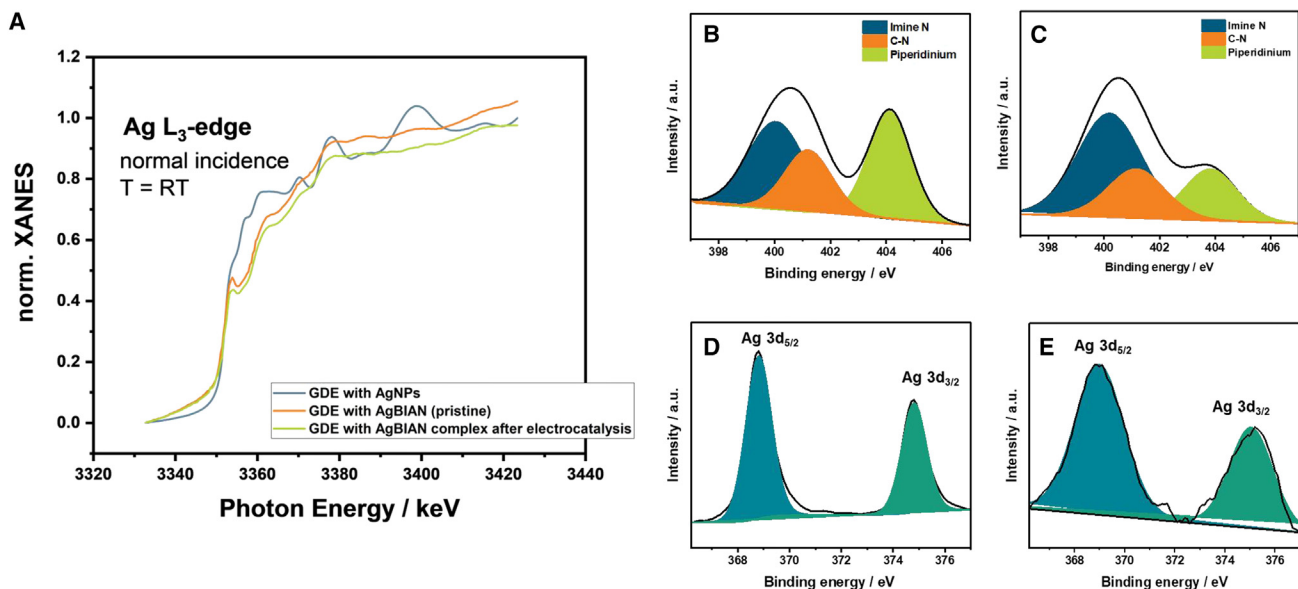


**Figure 3. Postmortem analysis of the 110-h tested GDEs at 300 mA cm<sup>-2</sup>**

(A) XANES investigation of a GDE coated with commercially available Ag-NPs against a pristine Ag-OC<sub>6</sub> GDE and long-term tested Ag-OC<sub>6</sub> GDE at 300 mA cm<sup>-2</sup> for 110 h.

(B and C) Obtained XPS spectra of the N-species of a pristine Ag-OC<sub>6</sub> GDE and long-term tested Ag-OC<sub>6</sub> GDE at 300 mA cm<sup>-2</sup> for 110 h.

(D and E) Obtained XPS spectra of the Ag species of a pristine Ag-OC<sub>6</sub> GDE and long-term tested Ag-OC<sub>6</sub> GDE at 300 mA cm<sup>-2</sup> for 110 h.

even after these harsh conditions, the L<sub>3</sub>-edge peak at 3,350 keV associated with Ag(I) species is still visible in our XANES spectra, albeit at decreased intensity, compared to a pristine Ag-BIAN electrode (Figure 3A).<sup>69,70</sup> This intensity decrease could be attributed to a loss of the Ag(I) species to Ag(0) but could also be the result of the delamination of the catalytic layer during the disassembling of the cell. Moreover, the respective Ag-XPS spectra and corresponding Auger parameters again show the existence of both Ag(0) and Ag(I) species. In this case, the balance is shifted again toward the metallic species. Regarding the BIAN-related spectra, also after 110 h of electrolysis, no significant changes can be observed compared to the pristine BIAN electrodes (Figures 3B–3D).

Although we do not believe that the Ag(I) species can be attributed to unused catalytic centers under such elevated current densities and electrolytic periods, the re-oxidation of the Ag center cannot be directly excluded.

Therefore, to gain an even clearer and direct insight regarding changes in the catalytic morphology, we also performed quasi-*in situ* XPS in 0.1 M KHCO<sub>3</sub> for all three Ag-BIAN complexes and Ag nanoparticles (Ag-NPs) at -2.0 V vs. Ag/AgCl for 1 h. Similarly to our previous observations, Ag-OC<sub>6</sub> and Ag-OMe show the emergence of a metallic phase after electrolysis at -2 V vs. Ag/AgCl. Interestingly, Ag-OC<sub>16</sub> remains oxidized after electrolysis, showing the critical role of electron-donating pendant groups on stabilizing the active metal center (Figure S45 and Table S11). Analyzing the Ag/N ratio provides a hint about the number of nitrogen atoms that are bound to Ag, thus indicating a loss of N sites or Ag sites by a decrease or increase of the number, respectively. An overall increase of the ratio was found after electrolysis, but to a decreasing degree as the alkyl chain was further elongated. Notably, while in the case of Ag-OMe the Ag/N changes significantly from 0.17 to 0.43 showing that the catalyst lies mainly in its metallic form, Ag-OC<sub>6</sub> and Ag-OC<sub>16</sub> do

not demonstrate such dramatic shifts, with the Ag/N ratios transitioning from 0.36 to 0.43 and 0.18 to 0.24, respectively ([Table S12](#)).

Overall, our *in situ* XPS results point to a ligand-dependent transformation of the different Ag-BIAN catalysts under electrolytic conditions. BIAN ligand with comparatively less electron-donating substituents, such as Ag-OMe, promotes the transformation to Ag-NPs. On the other hand, further increasing the current density close to the Ag center appears to assist its preservation in the Ag(I) state.

#### Are Ag-BIAN catalysts molecular or nanoparticle electrocatalysts?

Summarizing our postmortem analysis, we can conclude that our most attractive Ag-BIAN system, Ag-OC<sub>6</sub>, mainly forms a stabilized Ag(0)-BIAN species, accompanied by the existence of Ag(I) species. Here, we conclude that the active species during electrolysis correspond closer to Ag(0)-BIAN clusters rather than simply formed Ag-NPs, which would show a decreasing performance due to agglomeration. Notably, according to our *in situ* XPS results, in order to maintain the Ag(I)-BIAN catalysts in their molecular form the further elongation of the electron-donating alkyl chain as for Ag-OC<sub>16</sub> is required, though at the detriment of solubility and activity toward CO<sub>2</sub>R. This double-edged effect shows that GDE and catalyst optimization, especially of molecular-based ones, lie on a very fine balance.

To clearly understand whether the BIANs ligand truly assists during the CO<sub>2</sub>R cycle instead of simply stabilizing Ag-NPs, we mixed Ag-NPs with the free BIAN-OC<sub>6</sub> ligand in a 1:1 and 1:10 ratio, trying to approximate our most active Ag-OC<sub>6</sub> catalyst, maintaining our catalyst/carbon/Nafion electrode architecture. Interestingly, simple mixing of the two components leads to an FE<sub>CO</sub> improvement of 12% (FE<sub>CO</sub>: 77%) and 15% (FE<sub>CO</sub>: 81%) at 300 mA cm<sup>-2</sup> for the Ag/BIAN (1:10) and Ag/BIAN (1:1) hybrids, respectively, compared to our pristine Ag-NPs-coated GDE (FE<sub>CO</sub>: 65%). This is also accompanied by a small decrease in the cell voltage by 50–100 mV ([Figure S46](#)). These results possibly open interesting research opportunities toward tailoring organic ligand with metal NPs for ZGEs, ultimately circumventing issues with dissolution and demetallation of single-atom metal centers. Nevertheless, in comparison, the pristine Ag-OC<sub>6</sub> GDEs still outcompete their Ag-NP/BIAN analogs showing similar cell voltages. These control experiments thus show that: (1) BIAN ligands play an ameliorating role during CO<sub>2</sub>R, easily boosting the performance of metal electrocatalysts; (2) the active species generated via the Ag-OC<sub>6</sub> is significantly more active and tailored for the CO<sub>2</sub>R compared to simple catalyst-ligand mixing.

We herein present a series of N-co-coordinated Ag compounds based on the BIAN ligand scaffold and show their ability to constitute not only an efficient but also cost-sustainable alternative for the reduction of CO<sub>2</sub> in scalable electrolyzers. The Ag-BIAN presented here lies at the crossing point between molecular and nanoparticulate electrocatalysts, opening promising research opportunities to improve and understand not only the synthesis but also the ink composition and fabrication method of such novel systems. Notably, we also show that simple mixing of Ag-NPs with organic ligands can lead to notable performance improvements, opening collaboration pathways between academic and industrial partners toward the generation of tailored ligand-nanoparticle “hybrids” for CO<sub>2</sub> electroreduction under high-stress conditions.

In understanding the dynamic interaction of novel electrocatalysts with the operational conditions of the electrolyzer, using multiple reference electrodes and *operando* X-ray techniques will further strengthen our understanding of the underlying

operation and transformation mechanisms that such catalysts undergo. Finally, we hope that the toolkit and holistic pathway presented herein will help the community to improve both the activity and stability of the system in both industrially focused but also fundamental studies.

## EXPERIMENTAL PROCEDURES

### Resource availability

#### *Lead contact*

Further information and requests for resources should be directed to and will be fulfilled by the lead contact, Ulf-Peter Apfel ([ulf.apfel@rub.de](mailto:ulf.apfel@rub.de)), and corresponding author Wolfgang Schöfberger ([wolfgang.schoefberger@jku.at](mailto:wolfgang.schoefberger@jku.at))

#### *Materials availability*

All unique reagents generated in this study are available from the [lead contact](#) without restriction.

#### *Data and code availability*

All data supporting the findings can be found in the article and [supplemental information](#) or is available from the authors upon request. This study did not generate any computational datasets.

## SUPPLEMENTAL INFORMATION

Supplemental information can be found online at <https://doi.org/10.1016/j.xcpr.2023.101746>.

## ACKNOWLEDGMENTS

K.P. acknowledges the Funds of the Chemical Industry for a PhD Fellowship. S.A. and U.-P.A. were funded by the Deutsche Forschungsgemeinschaft (DFG, German Research Foundation) under Germany's Excellence Strategy - EXC 2033 - 390677874 - RESOLV as well as APAP242/9-1, and the Fraunhofer Internal Programs under grant no. Attract 097-602175. D.S. is grateful to BMBF for the financial support within the NanoMatFutur Project "H2Organic" no. 03XP0421. The authors are also thankful for support by the Mercator Research Center Ruhr (MERCUR.Exzellenz, "DIMENSION" Ex-2021-0034 and "KataSign" Ko-2021-0016). W.S. acknowledges the financial support of the Austrian Science Fund (FWF Standalone Projects P28167 "Heterogeneous catalysis for water oxidation and hydrogen evolution" and P32045 "Catalysts for biomass valorization") and of the Austrian Research Promotion Agency FFG ("CO<sub>2</sub>Val", FFG bridge project no. 883671). W.S. also acknowledges financial support by the Klima- und Energiefonds; the project is carried out within the framework of the "Energieforschungsprogramm 2022" (FFG project number: FO999903855).

## AUTHOR CONTRIBUTIONS

Conceptualization, K.P., D.K., H.S., K.J.P., D.S., B.R.C., W.S., and U.-P.A.; methodology, K.P., D.K., H.S., W.S., and U.-P.A.; investigation, K.P., D.K., C.R., H.S., H.A., L.S., S.A.S., L.H., and L.M.; visualization, K.P., D.K., H.S., S.A.S., L.H., and L.M.; funding acquisition, W.S. and U.-P.A.; project administration, W.S. and U.-P.A.; supervision, B.R.C., W.S., and U.-P.A.; writing – original draft, K.P., D.K., H.S., L.H., K.J.P., D.S., B.R.C., W.S., and U.-P.A.

## DECLARATION OF INTERESTS

The authors declare no competing interests.

## INCLUSION AND DIVERSITY

We support inclusive, diverse, and equitable conduct of research.

Received: July 31, 2023

Revised: October 16, 2023

Accepted: November 22, 2023

Published: December 13, 2023

## REFERENCES

- Lees, E.W., Mowbray, B.A.W., Parlance, F.G.L., and Berlinguette, C.P. (2021). Gas diffusion electrodes and membranes for CO<sub>2</sub> reduction electrolyzers. *Nat. Rev. Mater.* 7, 55–64.
- Luna, P. de, Hahn, C., Higgins, D., Jaffer, S.A., Jaramillo, T.F., and Sargent, E.H. (2019). What would it take for renewably powered electrosynthesis to displace petrochemical processes? *Science* (New York, N.Y.) 364,
- Bushuyev, O.S., De Luna, P., Dinh, C.T., Tao, L., Saur, G., van de Lagemaat, J., Kelley, S.O., and Sargent, E.H. (2018). What Should We Make with CO<sub>2</sub> and How Can We Make It? *Joule* 2, 825–832.
- Dinh, C.-T., García de Arquer, F.P., Sinton, D., and Sargent, E.H. (2018). High Rate, Selective, and Stable Electroreduction of CO<sub>2</sub> to CO in Basic and Neutral Media. *ACS Energy Lett.* 3, 2835–2840.
- Edwards, J.P., Alerte, T., O'Brien, C.P., Gabardo, C.M., Liu, S., Wicks, J., Gaona, A., Abed, J., Xiao, Y.C., Young, D., et al. (2023). Pilot-Scale CO<sub>2</sub> Electrolysis Enables a Semi-empirical Electrolyzer Model. *ACS Energy Lett.* 8, 2576–2584.
- Xu, Y., Edwards, J.P., Liu, S., Miao, R.K., Huang, J.E., Gabardo, C.M., O'Brien, C.P., Li, J., Sargent, E.H., and Sinton, D. (2021). Self-Cleaning CO<sub>2</sub> Reduction Systems: Unsteady Electrochemical Forcing Enables Stability. *ACS Energy Lett.* 6, 809–815.
- Endrődi, B., Kecsenovity, E., Samu, A., Darvas, F., Jones, R.V., Török, V., Danyi, A., and Janáky, C. (2019). Multilayer Electrolyzer Stack Converts Carbon Dioxide to Gas Products at High Pressure with High Efficiency. *ACS Energy Lett.* 4, 1770–1777.
- Endrődi, B., Samu, A., Kecsenovity, E., Halmágyi, T., Sebők, D., and Janáky, C. (2021). Operando cathode activation with alkali metal cations for high current density operation of water-fed zero-gap carbon dioxide electrolyzers. *Nat. Energy* 6, 439–448.
- Wang, R., Haspel, H., Pustovarenko, A., Dikhtirenko, A., Russikh, A., Shterk, G., Osadchii, D., Ould-Chikh, S., Ma, M., Smith, W.A., et al. (2019). Maximizing Ag Utilization in High-Rate CO<sub>2</sub> Electrochemical Reduction with a Coordination Polymer-Mediated Gas Diffusion Electrode. *ACS Energy Lett.* 4, 2024–2031.
- Ma, S., Lan, Y., Perez, G.M.J., Moniri, S., and Kenis, P.J.A. (2014). Silver supported on titania as an active catalyst for electrochemical carbon dioxide reduction. *ChemSusChem* 7, 866–874.
- Tornow, C.E., Thorson, M.R., Ma, S., Gewirth, A.A., and Kenis, P.J.A. (2012). Nitrogen-based catalysts for the electrochemical reduction of CO<sub>2</sub> to CO. *J. Am. Chem. Soc.* 134, 19520–19523.
- Masel, R.I., Liu, Z., Yang, H., Kaczur, J.J., Carrillo, D., Ren, S., Salvatore, D., and Berlinguette, C.P. (2021). An industrial perspective on catalysts for low-temperature CO<sub>2</sub> electrolysis. *Nat. Nanotechnol.* 16, 118–128.
- Garg, S., Li, M., Weber, A.Z., Ge, L., Li, L., Rudolph, V., Wang, G., and Rufford, T.E. (2020). Advances and challenges in electrochemical CO<sub>2</sub> reduction processes: an engineering and design perspective looking beyond new catalyst materials. *J. Mater. Chem. A*, 8, 1511–1544.
- Seteiz, K., Häberlein, J.N., Heizmann, P.A., Disch, J., and Vierrath, S. (2023). Carbon black supported Ag nanoparticles in zero-gap CO<sub>2</sub> electrolysis to CO enabling high mass activity. *RSC Adv.* 13, 18916–18926.
- Hoof, L., Thissen, N., Pellumbi, K., Junge Puring, K., Siegmund, D., Mechlér, A.K., and Apfel, U.-P. (2022). Hidden parameters for electrochemical carbon dioxide reduction in zero-gap electrolyzers. *Cell Reports Physical Science* 3, 100825.
- Reyes, A., Jansonius, R.P., Mowbray, B.A.W., Cao, Y., Wheeler, D.G., Chau, J., Dvorak, D.J., and Berlinguette, C.P. (2020). Managing Hydration at the Cathode Enables Efficient CO<sub>2</sub> Electrolysis at Commercially Relevant Current Densities. *ACS Energy Lett.* 5, 1612–1618.
- Ren, S., Joulié, D., Salvatore, D., Torbensen, K., Wang, M., Robert, M., and Berlinguette, C.P. (2019). Molecular electrocatalysts can mediate fast, selective CO<sub>2</sub> reduction in a flow cell. *Science* (New York, N.Y.) 365, 367–369.
- Gonglach, S., Paul, S., Haas, M., Pillwein, F., Sreejith, S.S., Barman, S., De, R., Mülegger, S., Gerschel, P., Apfel, U.-P., et al. (2019). Molecular cobalt corrole complex for the heterogeneous electrocatalytic reduction of carbon dioxide. *Nat. Commun.* 10, 3864.
- Grammatico, D., Bagnall, A.J., Riccardi, L., Fontecave, M., Su, B.-L., and Billon, L. (2022). Heterogenised Molecular Catalysts for Sustainable Electrochemical CO<sub>2</sub> Reduction. *Angew. Chem., Int. Ed. Engl.* 61, e202206399.
- Lv, X., Liu, Q., Yang, H., Wang, J., Wu, X., Li, X., Qi, Z., Yan, J., Wu, A., Cheng, T., and Wu, H.B. (2023). Nanoconfined Molecular Catalysts in Integrated Gas Diffusion Electrodes for High-Current-Density CO<sub>2</sub> Electroreduction. *Adv. Funct. Mater.* 33.
- Siritanarakul, B., Forster, M., Greenwell, F., Sharma, P.K., Yu, E.H., and Cowan, A.J. (2022). Zero-Gap Bipolar Membrane Electrolyzer for Carbon Dioxide Reduction Using Acid-Tolerant Molecular Electrocatalysts. *J. Am. Chem. Soc.* 144, 7551–7556.
- Chen, C., Liu, F.-S., and Szostak, M. (2021). BIAN-NHC Ligands in Transition-Metal-Catalysis: A Perfect Union of Sterically Encumbered, Electronically Tunable N-Heterocyclic Carbenes? *Chemistry* 27, 4478–4499.
- Hasan, K., Wang, J., Pal, A.K., Hierlinger, C., Guerchais, V., Sen Soo, H., García, F., and Zysman-Colman, E. (2017). Bay-Region Functionalisation of Ar-BIAN Ligands and Their Use Within Highly Absorptive Cationic Iridium(III) Dyes. *Sci. Rep.* 7, 15520.
- Wang, J., Ganguly, R., Yongxin, L., Diaz, J., Soo, H.S., and García, F. (2016). A multi-step solvent-free mechanochemical route to indium(iii) complexes. *Dalton Trans.* 45, 7941–7946. Cambridge, England : 2003.
- Wang, J., Soo, H.S., and García, F. (2020). Synthesis, properties, and catalysis of p-block complexes supported by bis(arylimino) acenaphthene ligands. *Commun. Chem.* 3, 113–13.
- Garg, S., Xu, Q., Moss, A.B., Mirolo, M., Deng, W., Chorkendorff, I., Drnec, J., and Seger, B. (2023). How alkali cations affect salt precipitation and CO<sub>2</sub> electrolysis performance in membrane electrode assembly electrolyzers. *Energy Environ. Sci.* 16, 1631–1643.
- Moss, A.B., Garg, S., Mirolo, M., Giron Rodriguez, C.A., Ilvonen, R., Chorkendorff, I., Drnec, J., and Seger, B. (2023). In operando investigations of oscillatory water and carbonate effects in MEA-based CO<sub>2</sub> electrolysis devices. *Joule* 7, 350–365.
- Ren, S., Lees, E.W., Hunt, C., Jewlal, A., Kim, Y., Zhang, Z., Mowbray, B.A.W., Fink, A.G., Melo, L., Grant, E.R., and Berlinguette, C.P. (2023). Catalyst Aggregation Matters for Immobilized

- Molecular CO<sub>2</sub>RR Electrocatalysts. *J. Am. Chem. Soc.* 145, 4414–4420.
29. Ren, S., Zhang, Z., Lees, E.W., Fink, A.G., Melo, L., Hunt, C., Dvorak, D.J., Yu Wu, W., Grant, E.R., and Berlinguet, C.P. (2022). Electrocatalysts Derived from Copper Complexes Transform CO into C<sub>2+</sub> Products Effectively in a Flow Cell. *Chemistry* 28, e202200340.
30. Weekes, D.M., Salvatore, D.A., Reyes, A., Huang, A., and Berlinguet, C.P. (2018). Electrolytic CO<sub>2</sub> Reduction in a Flow Cell. *Acc. Chem. Res.* 51, 910–918.
31. Bullock, R.M., Das, A.K., and Appel, A.M. (2017). Surface Immobilization of Molecular Electrocatalysts for Energy Conversion. *Chemistry* 23, 7626–7641.
32. Han, N., Wang, Y., Ma, L., Wen, J., Li, J., Zheng, H., Nie, K., Wang, X., Zhao, F., Li, Y., et al. (2017). Supported Cobalt Polyphthalocyanine for High-Performance Electrocatalytic CO<sub>2</sub> Reduction. *Chem. Mater.* 3, 652–664.
33. Nichols, E.M., Derrick, J.S., Nistanaki, S.K., Smith, P.T., and Chang, C.J. (2018). Positional effects of second-sphere amide pendants on electrochemical CO<sub>2</sub> reduction catalyzed by iron porphyrins. *Chem. Sci.* 9, 2952–2960.
34. Chapovetsky, A., Welborn, M., Luna, J.M., Haiges, R., Miller, T.F., and Marinescu, S.C. (2018). Pendant Hydrogen-Bond Donors in Cobalt Catalysts Independently Enhance CO<sub>2</sub> Reduction. *ACS Cent. Sci.* 4, 397–404.
35. Chen, K., Cao, M., Lin, Y., Fu, J., Liao, H., Zhou, Y., Li, H., Qiu, X., Hu, J., Zheng, X., et al. (2022). Ligand Engineering in Nickel Phthalocyanine to Boost the Electrocatalytic Reduction of CO<sub>2</sub>. *Adv. Funct. Mater.* 32, 2111322.
36. El-Ayaaan, U., Murata, F., El-Derby, S., and Fukuda, Y. (2004). Synthesis, structural and solvent influence studies on solvatochromic mixed-ligand copper(II) complexes with the rigid nitrogen ligand: bis[N-(2,4,6-trimethylphenyl)imino]acenaphthene. *J. Mol. Struct.* 692, 209–216.
37. Guo, L., Kong, W., Xu, Y., Yang, Y., Ma, R., Cong, L., Dai, S., and Liu, Z. (2018). Large-scale synthesis of novel sterically hindered acenaphthene-based  $\alpha$ -diimine ligands and their application in coordination chemistry. *J. Organomet. Chem.* 859, 58–67.
38. Khrizanforova, V.V., Fayzullin, R.R., Bogomyakov, A.S., Morozov, V.I., Batulin, R.G., Gerasimova, T.P., Islamov, D.R., and Budnikova, Y.H. (2023). Cobalt(II) Coordination to an N4-Acenaphthene-Based Ligand and its Sodium Complex (Cambridge, England: Dalton transactions).
39. Buckley, A.K., Ma, S., Huo, Z., Gao, T.Z., and Kuhl, K.P. (2022). Nanomaterials for carbon dioxide conversion at industrial scale. *Nat. Nanotechnol.* 17, 811–813.
40. Wu, X., Sun, J.W., Liu, P.F., Zhao, J.Y., Liu, Y., Guo, L., Dai, S., Yang, H.G., and Zhao, H. (2022). Molecularly Dispersed Cobalt Phthalocyanine Mediates Selective and Durable CO<sub>2</sub> Reduction in a Membrane Flow Cell. *Adv. Funct. Mater.* 32, 2107301.
41. Yue, Z., Ou, C., Ding, N., Tao, L., Zhao, J., and Chen, J. (2020). Advances in Metal Phthalocyanine based Carbon Composites for Electrocatalytic CO<sub>2</sub> Reduction. *ChemCatChem* 12, 6103–6130.
42. Gotico, P., Halime, Z., and Aukauloo, A. (2020). Recent advances in metalloporphyrin-based catalyst design towards carbon dioxide reduction: from bio-inspired second coordination sphere modifications to hierarchical architectures. *Dalton Trans.* 49, 2381–2396. Cambridge, England : 2003.
43. Zhao, J., Lyu, H., Wang, Z., Ma, C., Jia, S., Kong, W., and Shen, B. (2023). Phthalocyanine and porphyrin catalysts for electrocatalytic reduction of carbon dioxide: Progress in regulation strategies and applications. *Separ. Purif. Technol.* 312, 123404.
44. Zhao, S., Jin, R., and Jin, R. (2018). Opportunities and Challenges in CO<sub>2</sub> Reduction by Gold- and Silver-Based Electrocatalysts: From Bulk Metals to Nanoparticles and Atomically Precise Nanoclusters. *ACS Energy Lett.* 3, 452–462.
45. Bernauer, J., Pölker, J., and Jacobi von Wangenheim, A. (2022). Redox-active BIAN-based Diimine Ligands in Metal-Catalyzed Small Molecule Syntheses. *ChemCatChem* 14, e202101182.
46. Costentin, C., Drouet, S., Robert, M., and Savéant, J.M. (2012). A local proton source enhances CO<sub>2</sub> electroreduction to CO by a molecular Fe catalyst. *Science (New York, N.Y.)* 338, 90–94.
47. Costentin, C., Passard, G., Robert, M., and Savéant, J.M. (2014). Ultraefficient homogeneous catalyst for the CO<sub>2</sub>-to-CO electrochemical conversion. *Proc. Natl. Acad. Sci. USA* 111, 14990–14994.
48. Zhang, X., Wang, Y., Gu, M., Wang, M., Zhang, Z., Pan, W., Jiang, Z., Zheng, H., Lucero, M., Wang, H., et al. (2020). Molecular engineering of dispersed nickel phthalocyanines on carbon nanotubes for selective CO<sub>2</sub> reduction. *Nat. Energy* 5, 684–692.
49. Wang, M., Torbensen, K., Salvatore, D., Ren, S., Joulié, D., Dumoulin, F., Mendoza, D., Lassalle-Kaiser, B., Işci, U., Berlinguet, C.P., and Robert, M. (2019). CO<sub>2</sub> electrochemical catalytic reduction with a highly active cobalt phthalocyanine. *Nat. Commun.* 10, 3602.
50. Vass, Á., Kormányos, A., Kószó, Z., Endrődi, B., and Janáky, C. (2022). Anode Catalysts in CO<sub>2</sub> Electrolysis: Challenges and Untapped Opportunities. *ACS Catal.* 12, 1037–1051.
51. Vass, Á., Endrődi, B., Samu, G.F., Balog, Á., Kormányos, A., Cherevko, S., and Janáky, C. (2021). Local Chemical Environment Governs Anode Processes in CO<sub>2</sub> Electrolyzers. *ACS Energy Lett.* 6, 3801–3808.
52. El-Nagar, G.A., Haun, F., Gupta, S., Stojkovic, S., and Mayer, M.T. (2023). Unintended cation crossover influences CO<sub>2</sub> reduction selectivity in Cu-based zero-gap electrolyzers. *Nat. Commun.* 14, 2062.
53. Endrődi, B., Kecsenovity, E., Samu, A., Halmágyi, T., Rojas-Carbonell, S., Wang, L., Yan, Y., and Janáky, C. (2020). High carbonate ion conductance of a robust PiperION membrane allows industrial current density and conversion in a zero-gap carbon dioxide electrolyzer cell. *Energy Environ. Sci.* 13, 4098–4105.
54. Samu, A.A., Szentí, I., Kukovecz, Á., Endrődi, B., and Janáky, C. (2023). Systematic screening of gas diffusion layers for high performance CO<sub>2</sub> electrolysis. *Commun. Chem.* 6, 41.
55. Subramanian, S., Yang, K., Li, M., Sassenburg, M., Abdinejad, M., İrem, E., Middelkoop, J., and Burdyny, T. (2023). Geometric Catalyst Utilization in Zero-Gap CO<sub>2</sub> Electrolyzers. *ACS Energy Lett.* 8, 222–229.
56. Haas, T., Krause, R., Weber, R., Demler, M., and Schmid, G. (2018). Technical photosynthesis involving CO<sub>2</sub> electrolysis and fermentation. *Nat. Catal.* 1, 32–39.
57. Wei, P., Li, H., Li, R., Wang, Y., Liu, T., Cai, R., Gao, D., Wang, G., and Bao, X. (2023). The Role of Interfacial Water in CO<sub>2</sub> Electrolysis over Ni-N-C Catalyst in a Membrane Electrode Assembly Electrolyzer. *Small (Germany: Weinheim an der Bergstrasse)*, pp. e2300856.
58. Shin, H., Hansen, K.U., and Jiao, F. (2021). Techno-economic assessment of low-temperature carbon dioxide electrolysis. *Nat. Sustain.* 4, 911–919.
59. Moore, T., Oyarzun, D.I., Li, W., Lin, T.Y., Goldman, M., Wong, A.A., Jaffer, S.A., Sarkar, A., Baker, S.E., Duoss, E.B., and Hahn, C. (2023). Electrolyzer energy dominates separation costs in state-of-the-art CO<sub>2</sub> electrolyzers: Implications for single-pass CO<sub>2</sub> utilization. *Joule* 7, 782–796.
60. Heßmann, M., Minten, H., Geissler, T., Keller, R.G., Bardow, A., and Wessling, M. (2023). Why Membranes Matter: Ion Exchange Membranes in Holistic Process Optimization of Electrochemical CO<sub>2</sub> Reduction. *Advanced Sustainable Systems* 7.
61. Cofell, E.R., Nwabara, U.O., Bhargava, S.S., Henckel, D.E., and Kenis, P.J.A. (2021). Investigation of Electrolyte-Dependent Carbonate Formation on Gas Diffusion Electrodes for CO<sub>2</sub> Electrolysis. *ACS Appl. Mater. Interfaces* 13, 15132–15142.
62. Kutz, R.B., Chen, Q., Yang, H., Sajjad, S.D., Liu, Z., and Masel, I.R. (2017). Sustainion Imidazolium-Functionalized Polymers for Carbon Dioxide Electrolysis. *Energ. Tech.* 5, 929–936.
63. Sarma, S.C., Barrio, J., Bagger, A., Pedersen, A., Gong, M., Luo, H., Wang, M., Favero, S., Zhao, C.-X., Zhang, Q., et al. (2023). Reaching the Fundamental Limitation in CO<sub>2</sub> Reduction to CO with Single Atom Catalysts. *Adv. Funct. Mater.* 33.
64. Zhou, Y., Zhou, Q., Liu, H., Xu, W., Wang, Z., Qiao, S., Ding, H., Chen, D., Zhu, J., Qi, Z., et al. (2023). Asymmetric dinitrogen-coordinated nickel single-atomic sites for efficient CO<sub>2</sub> electroreduction. *Nat. Commun.* 14, 3776.

65. Boutin, E., and Robert, M. (2021). Molecular Electrochemical Reduction of CO<sub>2</sub> beyond Two Electrons. *Trends in Chemistry* 3, 359–372.
66. Tarrago, M., Ye, S., and Neese, F. (2022). Electronic structure analysis of electrochemical CO<sub>2</sub> reduction by iron-porphyrins reveals basic requirements for design of catalysts bearing non-innocent ligands. *Chem. Sci.* 13, 10029–10047.
67. Queyriaux, N., Abel, K., Fize, J., Pécaut, J., Orio, M., and Hammarström, L. (2020). From non-innocent to guilty: on the role of redox-active ligands in the electro-assisted reduction of CO<sub>2</sub> mediated by a cobalt(II)-polypyridyl complex. *Sustain. Energy Fuels* 4, 3668–3676.
68. Franco, F., Rettenmaier, C., Jeon, H.S., and Roldan Cuenya, B. (2020). Transition metal-based catalysts for the electrochemical CO<sub>2</sub> reduction: from atoms and molecules to nanostructured materials. *Chem. Soc. Rev.* 49, 6884–6946.
69. Behrens, P. (1992). Bonding in silver-oxygen compounds from Ag L3 XANES spectroscopy. *Solid State Commun.* 81, 235–239.
70. Bovenkamp, G.L., Zanzen, U., Krishna, K.S., Hormes, J., and Prange, A. (2013). X-Ray Absorption Near-Edge Structure (XANES) Spectroscopy Study of the Interaction of Silver Ions with *Staphylococcus aureus*, *Listeria monocytogenes*, and *Escherichia coli*. *Appl. Environ. Microbiol.* 79, 6385–6390.